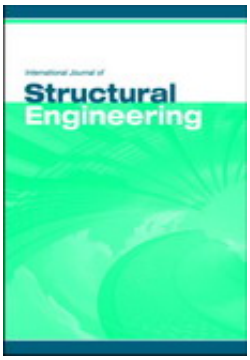

International Journal of Structural Engineering

ISSN online: 1758-7336 - ISSN print: 1758-7328
https://www.inderscience.com/ijstructe

Study of the influence of water saturation on main mechanical properties of laterite dimension stones from Burkina Faso

Hassane Seini Moussa, Abdou Lawane, Decroly Djoubissié Denouwé

DOI: 10.1504/IJSTRUCTE.2025.10069072

Article History:

Received:	04 October 2023
Last revised:	29 January 2024
Accepted:	31 January 2024
Published online:	10 February 2025

Study of the influence of water saturation on main mechanical properties of laterite dimension stones from Burkina Faso

Hassane Seini Moussa*, Abdou Lawane and Decroly Djoubissié Denouwé

Laboratoire Eco-matériaux et Habitats Durables (LEMHaD),
Institut International d'Ingénierie de l'Eau et de l'Environnement (2iE),
01 BP 594 Ouagadougou 01, Burkina Faso
Email: hassane.seini@2ie-edu.org
Email: abdou.lawane@2ie-edu.org
Email: decroly.djoubissie@2ie-edu.org
*Corresponding author

Abstract: This scientific paper presents the findings of a study on the hydromechanical behaviour of laterite stones (LS) from four quarries in Burkina Faso. The study examines the impact of water saturation on the compressive strength, tensile strength, Young modulus, and Poisson's ratio of the stones. The results indicate that water saturation significantly reduces the mechanical characteristics of the stones, with up to a 71% decrease in compressive strength and a 61% decrease in Young modulus. The study also highlights the influence of pore size and distribution on strength loss and identifies correlations between physical and mechanical properties under dry and saturated conditions. Furthermore, it reveals that the behaviour of LS varies depending on block size, with large blocks exhibiting brittle behaviour and smaller blocks showing ductile behaviour. The study also discusses the influence of the hydric state on the behaviour change of the stones. Additionally, it identifies novel correlation functions between mechanical and physical properties under dry and saturated conditions, which can provide an alternative to costly laboratory experiments. The study offers valuable insights into the mechanical behaviour of stones under different hydric states and provides practical implications for selecting and using stone materials in various environments.

Keywords: influence of water; mechanical properties; laterite stone; Burkina Faso.

Reference to this paper should be made as follows: Seini Moussa, H., Lawane, A. and Djoubissié Denouwé, D. (2025) 'Study of the influence of water saturation on main mechanical properties of laterite dimension stones from Burkina Faso', *Int. J. Structural Engineering*, Vol. 15, No. 1, pp.1–28.

Biographical notes: Hassane Seini Moussa is a PhD student in Civil and Structural Engineering at Institut 2iE, specialising in laterite stone mosonry structures. His research focuses on understanding the material properties and performance of laterite, a locally sourced construction material, in response to environmental conditions. He has published several papers in peer-reviewed journals and presented his findings at international conferences, contributing to the knowledge base surrounding sustainable building practices. He holds a Master's in Structural Engineering from Institut 2iE and is passionate about promoting eco-friendly construction solutions that leverage indigenous resources while ensuring structural integrity and safety.

Abdou Lawane is an Associate Professor of Civil and Structural Engineering at Institut 2iE, focuses on earthen construction materials and recycling industrial wastes in sustainable building practices. With over ten years of experience, he has significantly contributed in innovative methods to enhance the performance of earth-based materials while minimising environmental impact. He has authored numerous publications in reputable journals and has been a keynote speaker at various international conferences. He actively collaborates with industry partners to promote greener construction techniques, aiming to bridge the gap between academia and practical applications for sustainable development in the construction sector.

Decroly Djoubissié Denouwé is an Assistant Professor in Civil and Structural Engineering at Institut 2iE, specialising in sustainable construction materials and the structural design of civil constructions. His research focuses on developing innovative, eco-friendly materials and methodologies that enhance the durability and sustainability of infrastructure. With a PhD in Structural Engineering, he has published several papers in leading journals and is acknowledged for his contributions to sustainable design practices. He is actively involved in interdisciplinary projects aimed at integrating sustainable solutions into urban development and infrastructure design, promoting an environmentally responsible approach to modern engineering challenges.

1 Introduction

Many studies conducted in various areas of the world have found that humidity negatively influences the mechanical properties of masonry materials (Kasthurba et al., 2007; Narayanaswamy et al., 2016; Nasheed et al., 2018). Previous and ongoing studies have largely shown its effects on structures' durability and safe dimensioning factors, especially concerning natural stones with high open porosity (Lawane Gana, 2014). Laterite dimension stone (LS) is known in tropical countries to be used for construction purposes. Laterite is a very common material in West African countries such as Burkina Faso. This material is cheap, but the little information available for predicting its mechanical behaviour slows its massive use for building. Because of incertitude, it is only used as filling material for buildings. Updating the definition given by Gidigasu forty years ago, Mvindi and Oyelami described the term laterite as a reddish ferruginous, vesicular, unstratified, and porous material with yellow ochers (Ndzié Mvindi et al., 2017; Oyelami and Van Rooy, 2016). It is a relatively soft material extracted manually or mechanically with pickaxes or saws. When exposed to air and sun effects, it hardens and becomes relatively resistant to weather effects (Lawane Gana, 2014). Laterite is a metasomatic stone formed in hot, humid tropical areas rich in iron and aluminium. It forms because of extensive and long-term weathering of the underlying parent stone (Kasthurba et al., 2007). Metasomatism is a metamorphic process in which the chemical composition of a stone is altered, involving the introduction or removal of chemical components due to the stone's interaction with its environment. Stones retain their solid state during the metasomatism process.

Many standards used to simulate aging on natural stones involve water, which, combined with other factors, indirectly induces weathering: thermal shock. However, the evolution of mechanical properties due to weathering cycles and moisture conditions are related to the ones in the dry state. Although the weather will surely affect the mechanical

properties, only the evolution of mechanical properties regarding the moisture conditions will be evaluated in this study.

Historically, Török has pointed out the dependence of mechanical behaviour on the water content of a porous stone (Török and Vásárhelyi, 2010). Porous stone behaves completely differently in a dry state than in a saturated state. It is stated that the water in the pore softens the bonding strength, and water adsorbed in small pores can be considered like osmotic fluids, which cause expansive and, ultimately, destructive forces in the stone (Rossana and Paola, 2012). Regarding the fluid dynamic through porous construction materials, some studies have given interesting information about the causes and consequences of the interaction between the construction material and the surrounding fluids. Xiaojie Sun et al. have studied and given computational mass transport methods in concrete under stress and crack conditions (Sun et al., 2023). They have clearly stated the influence of cracks in fluid transportation through the material but focus on the fluid in their gas forms, not the liquid. Depending on the stress condition and the cracks in the materials, the moisture transportation capacity depends on the crack width through a parabolic function relation. There are no similar studies that have deeply analysed this concern for LS. This study will try to do so. In addition, the mean capillary pore radius will be estimated through empirical formulas based on sorptivity values, and their influence on liquid water transportation and mechanical properties will be evaluated. Regarding the particle size distribution (PSD), even though it is not one of the main purposes of this study, it is important to notice that many studies have given methods for evaluating the radius and distribution of vapour-accessible pores in artificial materials and natural stones (Gong et al., 2014; Oguchi and Yu, 2021; Gong et al., 2022a; 2022b).

Since it is quite difficult to experiment on walls in saturated states, finding an alternative method that approaches those experimental results will be interesting. Many authors have proposed correlations between mechanical properties in saturated and dry conditions. Most have focused on compression strength only (Oguchi and Yu, 2021; Přikryl, 2013; Wong et al., 2016; Rossana and Paola, 2012) and rarely address other properties. Formulas and correlations shared in that paper do not sometimes fit the behaviour of LS since they have been developed on other masonry elements. Calculation formulas developed for other masonry elements, as for dimensioning, cannot be used for LS (Kabore et al., 2019).

The general objective of this study is to set methods and equations for assuming the stress and strain in laterite stone, considering the water saturation rate and the size of the stone. For achieving this aim, a couple of specific aims are stated, such as determining the main mechanical and physical properties of the laterite stone, analysing similarities and differences between quarries, highlighting trends in the behaviour of the LS regarding the size of the LS and its moisture content and finally setting methods or formulas for assessing the stress-strain curve of LS depending on their size and saturation rate.

In most cases, mechanical properties such as the modulus of elasticity and Poisson's ratio of building blocks are not tested when modelling masonry units or structures. Many numerical studies assume those values for laterite stone based on similar stone values or by interpolation on concrete's values. However, the modulus of elasticity and Poisson's ratio would be required in finite element modelling.

The present study used detailed laboratory experiments and mathematical analysis to assume or evaluate the behaviour of LS depending on moisture content evolution and

size. Those equations would be useful for future numerical modelling of the behaviour of masonry structures with LS.

2 Materials and methods

2.1 Description of LS and preparation of samples

Three quarries were identified in southwestern Burkina Faso and one in the outskirts of the city of Ouagadougou. Samples were collected from each. The LS are raw earthen materials, reddish-coloured, extracted from the localities of Kamboinsin, Dano, and Diebougou from four different. The laterite stone extracted from the quarry of Dano 1 is mechanically sawed, and the ones from the other quarries are handy and pulled with pickaxes. The information on their coordinates and the extraction mode are presented in Figure 1 and Table 1. Figure 2 presents the photographic views of the quarries and the LS. The specifications for the masonry units were chosen according to NF EN 771-6 + A1 (2015). After collecting the LS, the sampled units were fit to regular dimensions with a saw according to the related French standards (NF EN 772-16, 2011; NF EN 13373, 2020).

Table 1 Coordinates of the quarries studied

Name of the quarry	*Latitude*	*Longitude*	*Altitude (m)*
DANO 1 (CERMA quarry)	11° 8’38.20’’N	3° 3’59.50’’W	322
DANO 2 (MENA quarry)	11° 10’29.14’’	3° 2’32.78’’W	278
DIEBOUGOU (MALO quarry)	10° 58’43.19’’N	3°14’12.38’’W	295
KAMBOINSIN	12° 26’ 48’’ N	1° 33’ 45’’ W	301

Figure 1 Location of the quarries on the map of Burkina Faso (see online version for colours)

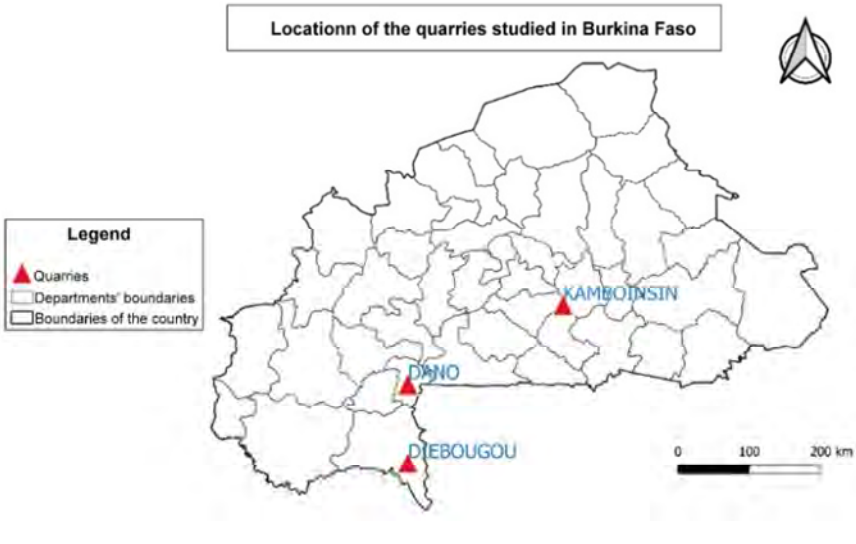

2.2 Compressive and flexural strength of laterite stone

LS were dried at 70±2°C until reaching constant mass. For measurements of the compressive strength or elastic modulus in a saturated state, samples used for tests will be immersed in water at least 48 hours before the test. During the process, the samples will be often weighed until the confirmation that the test reaches a constant saturated mass. All the mechanical properties, such as compressive strength, flexural strength, young modulus, and Poisson's ratio, were measured using a hydraulic press (Proeti safr, Madrid, Spain) equipped with a 300 kN capacity load cell at a loading rate of 0.05 mm/s. Five millimetres range LVDT sensors were used to measure deformations on the loaded samples. The compressive strength of a laterite block was determined using the guidelines of the French standards (NF EN 772-1 + A1, 2015; NF EN 1926, 2007). The experimental device is presented in Figure 3(a). The loading directions are presented in Figure 5 and Figure 6. The flexural tensile strength of a laterite block was determined using the guidelines of the standard (NF EN 12372, 2022). The experimental device is presented in Figure 3(b). The mentioned standard tested six to ten samples for each test. For comparison reasons, samples have been sized to 70 mm × 70 mm × 70 mm and 140 mm × 140 mm × 140 mm for compression tests. They were also loaded in the plan parallel to the bedding of the formation layers and the other plan perpendicular to the bedding of the formation layers.

Figure 2 Extraction mode on the quarries: (a) and (c) mechanically sawed, (b) and (d) manually (see online version for colours)

Figure 3 (a) Experimental devise for compression strength and (b) Flexural strength tests (see online version for colours)

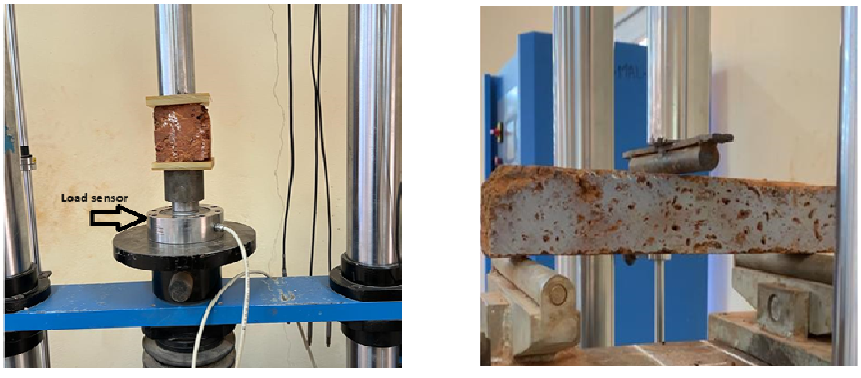

(a) (b)

2.3 Modulus of elasticity and Poisson's ratio of laterite stone

As stated for the first specific aim, part of this study attempts to find the modulus of elasticity and Poisson's ratio of laterite stone. The Poisson's ratio is calculated using equation (1) and Figure 4 on the same measurement range as the elastic modulus.

$$v = \frac{\varepsilon_H / l_0}{\varepsilon_V / L} \tag{1}$$

ε_H horizontal strain (mm)

ε_V vertical strain (mm)

l_0 height of the sample (mm)

L Width of the sample (mm).

Figure 4 Test device for determination of Poisson's ratio

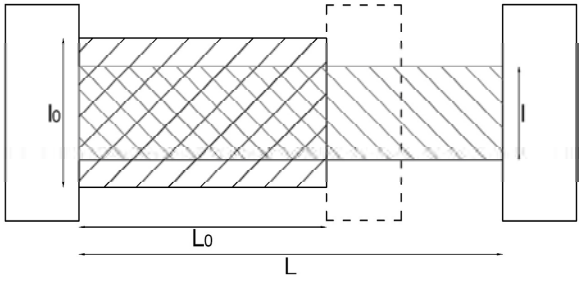

Figure 5 (a) and (b) Test device for determination of Poisson's ratio

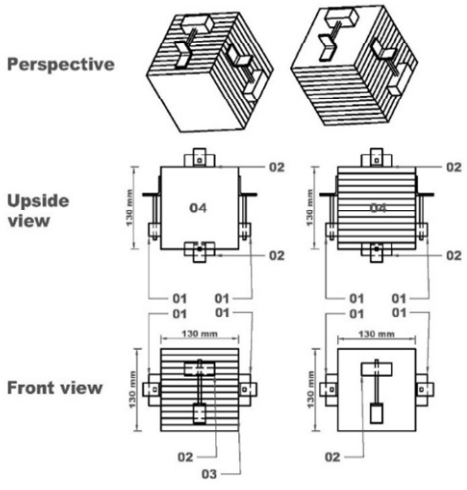

(a) (b)

Since Poisson's ratio links strains in perpendicular directions, placing LVDT in vertical and horizontal directions was necessary. Samples of dimensions of 130 × 130 × 130 cubic millimetres have been prepared to determine the Poisson's ratio. The test method is presented in Figure 5. The measurement range is the same as for the elastic modulus test. The modulus of elasticity was determined according to the standard NF EN 14580 (2005). The test method is presented in Figure 6.

Figure 6 (a) and (b) Test device for determination of elastic moduli

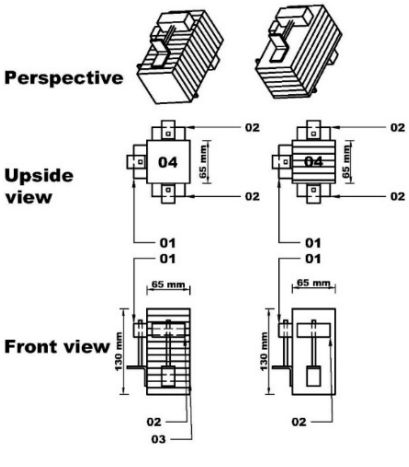

(a) (b)

Notes: 01: Horizontal strain measurement LVDT.
02: Vertical strain measurement LVDT.
03: Anisotropy plans
04: Loaded surface.

2.4 Physical characteristics

2.4.1 Capillary absorption

Whatever the civil engineering construction project is, it is affected by its environment, principally the water and humidity content. It is through absorption that a liquid can migrate from the outside to the inside of a porous material due to capillarity. The capillary absorption test determines the quantity of water absorbed by the capillarity of the samples. Several interesting LS characterisation parameters can be deduced from this value over time. The tests were conducted on LS samples using the protocol explained in the related French standards (NF EN 772-11, 2011; NF EN 1925, 1999). They measure the increase in the mass of the test specimen placed in a container whose water level is approximately 1 cm above the underside of the sample.

Sorptivity represents the rate of water absorption by capillarity. This parameter makes it possible to approximate the capillary pores' mean diameter accurately. From Washburn's theory of dynamic impregnation (Washburn, 1921), the relation of the equation below established by Cassagnabère et al. (2011), sorptivity (S) depends on the total porosity of the material and its average radius of the capillary pores.

$$S \times \sqrt{t} = \sqrt{\frac{\sigma \times r \times \cos\theta \times t}{2\mu}} \times p_0 \times \Phi_0 \tag{2}$$

S is the sorptivity (kg.m^{-2} h$^{-1/2}$)

t time laps (h)

σ the surface tension water (Pa)

r the average capillary pore radius (m)

θ angle of contact (°)

Φ_0 the density of the absorbed fluid (kg.m^{-3})

p_0 the total porosity of the specimen

μ the viscosity of water (Pa.s).

We deduce the average diameter of the pores r by the relation:

$$r = S^2 \times \frac{2\mu}{\sigma \times \cos\theta \times P_0^2 \times \Phi_0^2} \tag{3}$$

The mean temperature of the test conditions is 35±5°C.

2.4.2 Total water absorption test

The test consists of completely immersing the LS bloc in a liquid of known density, usually water, to saturate the pores. The mass gains are then measured by successive weighing in given time laps and until the sample is completely saturated. Of course, the LS must stay in contact with water for a long time to validate the measurements. These total water absorption tests were carried out according to standard (NF EN 1936, 2007; NF EN 13755, 2008) on LS blocks.

2.4.3 Porosity and density

The specific particle density of the materials is determined using a gas pycnometer according to the standard (D5550-6, 2015).

The gas pycnometer comprises two main elements: the tank and the assemblage of a pump + pressure gauge + pre-chamber. The tank, with a capacity of 1,000 cm^3, is filled with the material of which some physical characteristics are to be determined (density, water content, and air content).

The assemblage of the pump + manometer is used to pressurise a pre-chamber. The manometer indicates the pressure of this volume in meters of seawater. This pre-chamber is linked to the tank's volume via a valve operated by a lever: when the valve is open, the air pressure in the chamber is the same as the air pressure in the tank: the pressure gauge indicates the air pressure in the tank.

The valves nullify the pressures of the chamber and the tank. The hermetic connection between the tank and the measuring devices is ensured by an O-ring, the collar of the tank, and the correct closing of the screws.

Often noted ε_{tot} expressed in percentage of the volume (%), the porosity is a physical parameter of the samples, which in this case will be determined according to the standard (NF EN 1936, 2007). The method consists of the saturation of the porous matrix of the samples with a liquid of known density. In this case, water was used. Then, each sample will be weighed.

2.5 Statistical analysis of the results

A global overview of the quarries' results will be given by analysing the output results of the data mining software R combined with its plug-in R-studio. This dataset contains four individuals and 12 variables. The individuals are the quarries, and the variables are the measured properties (parameters). To facilitate the reading of the graphs, the information will be coded as follows:

Table 2 Codification of parameters for the statistical analysis

Parameter	*Code*	*Unit/dimension*
Unconfined compressive strength in dry state by loading in the direction perpendicular to the anisotropy plans	PRD	Mpa
Unconfined compressive strength in dry state by loading in the direction parallel to the anisotropy plans	PPD	Mpa
Unconfined compressive strength in the saturated state by loading in the direction perpendicular to the anisotropy plans	PRS	Mpa
Unconfined compressive strength in saturated state by loading in the direction parallel to the anisotropy plans	PPS	Mpa
Mean capillary pore diameter distributed in the direction perpendicular to the anisotropy plans	CPDS1	µm
Mean capillary pore diameter distributed in the direction parallel to the anisotropy plans	CPDS2	µm
Total porosity	TPOR	%
Open porosity	OPOR	%
Mean absolute dry density	ADD	kg/m^3

Table 2 Codification of parameters for the statistical analysis (continued)

Parameter	*Code*	*Unit/dimension*
Mean indirect tensile strength	ITS	Mpa
Mean young modulus by loading in the direction perpendicular to the anisotropy plans	YMDS1	Mpa
Mean young modulus by loading in the direction parallel to the anisotropy plans	YMDS2	Mpa

Table 3 Codification of the quarries for the statistical analysis

Quarry	*Code*
Dano 1	DN1
Dano 2	DN2
Kamboinsin	KBS
Diébougou	DBG

Principal component analysis (PCA) will be conducted to reduce the number of dimensions of the study.

3 Results and discussion

3.1 Physical characteristics

The bulk and dry absolute density of the laterite stone variants ranged from 16 to 22 kN/m^3 and 24 to 29 kN/m^3, respectively. The Dano 1 stone had the highest bulk density value (22 kN/m3), whereas the Dano 2 stone had the lowest (16 kN/m3). In addition, the Dano 1 stone had the highest value absolute density (29 kN/m3), and Diebougou had the lowest value (24 kN/m^3). Figure 7 summarises the values of the density of each stone.

Figure 7 Graph of bulk and absolute dry density (see online version for colours)

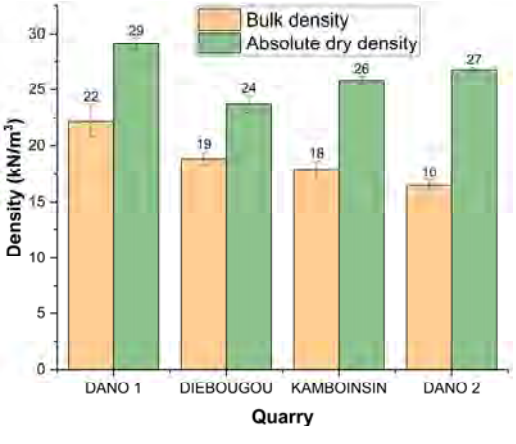

Figure 8 Graph of porosity values and saturation content rate (see online version for colours)

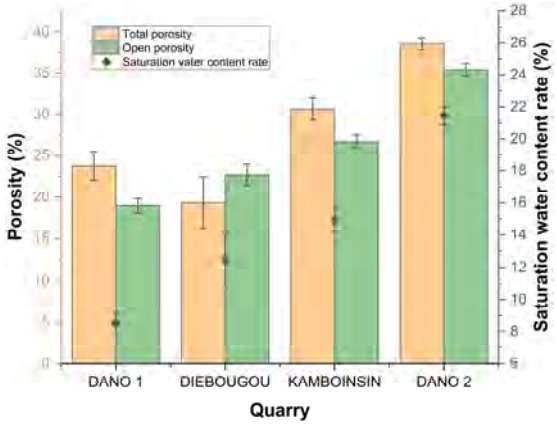

Figure 8 presents the values of the total open porosity of each stone. The LS of Dano 2 had the highest values, 38.50%, and 35.41%, respectively, for the total open porosity. LS from Diebougou had the lowest values. LS from Dano and Kamboinsin resist much better water exposition than the ones from Diebougou. Furthermore, after an immersion of two hours, coarse solid particles of stones of Diebougou detach and induce a relatively high standard deviation value, which sensitively affects equations that consider total porosity values. However, the other quarries are globally giving the general trend consistently.

Figure 9 Capillary absorption in direction 1 (parallel to anisotropy plans) (see online version for colours)

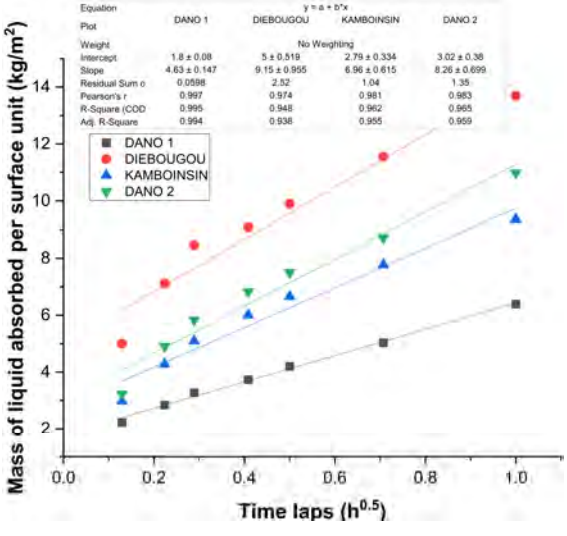

Regarding Figure 7 and Figure 8, a strong correlation between density and porosity values can be established. It is remarkable that the higher the total porosity value is, the lower the bulk density value is. It can also be noted that the saturation water content rate varies inversely proportional to bulk density values. Furthermore, Kamboinsin and Dano

2 have the same absolute dry density values sensitively. The inversion of the trend regarding bulk density values can be explained by the total porosity values of these stones since Dano 2 has higher porosity values than Kamboinsin. The observations in Figure 24 support Figure 24 those conclusions.

Figure 10 Capillary absorption in direction 2 (perpendicular to anisotropy plans)

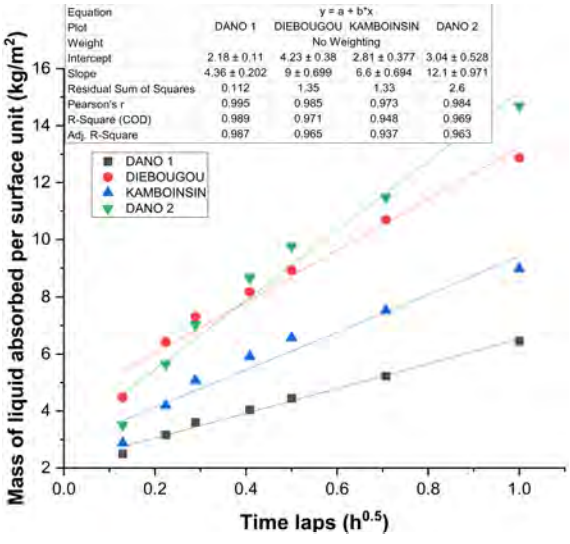

Figure 9 and Figure 10 present the capillary absorption scatter plots of the LS for each quarry. A linear regression curve is also presented for each scatter plot. The equation of each line and the statistical regressions' representation quality are given. The slope coefficient of the line indicates the value of the sorptivity of the LS, which somehow expresses the velocity of the absorption dynamic.

Figure 11 Average capillary pore diameters in parallel and perpendicular directions (see online version for colours)

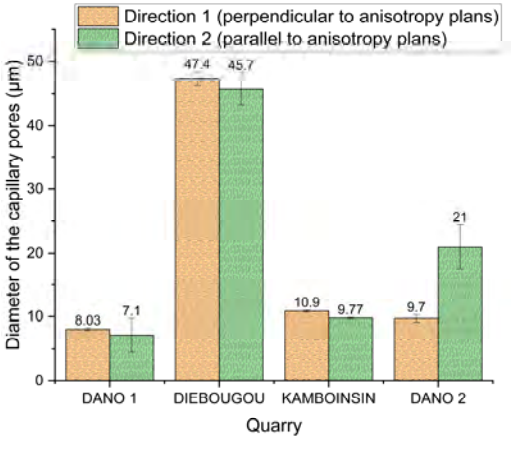

Globally, from one direction to another, all the quarries maintain the same trends except Dano 2, which presents a significant difference in sorptivity values. That implies that for stones from Dano 2, capillary pores absorb water or vapour faster in the direction perpendicular to anisotropy plans than in the direction parallel to anisotropy plans, and the other quarries studied maintain globally the same values regardless of the direction of exposition. That should be a consequence of the size and shape of the pores.

Regarding pore size distributions, Figure 11 revealed that stones from Diebougou have the highest pores' diameter (mainly between 45 and 48 µm). In contrast, stones from Dano 1 have the lowest pores' diameter (between 7 and 8 µm). Most stones studied have the same pores' diameter value sensitively in perpendicular and parallel directions, except those from Dano 2. It implies that except stones from Dano 2, all the stones have quite spherical pores, whereas Dano 2 has oval and flattened ones. According to the capillary absorption regression curves, the pores' distributions are regular all over the materials. However, the values of the standard deviation (std) observed and represented by the error bars should be highlighted since it can be observed that the std values are lower for sorptivity regarding the plans perpendicular to anisotropy plans than for the second direction. This phenomenon should be explained by the presence of cracks preferentially distributed in interfaces of sedimentation layers during the stone's geological history.

3.2 Mechanical characteristics

Figure 12 presents the unconfined compression strength (UCS) of the LS regarding the water content of the samples.

Figure 12 Unconfined compression strength (UCS) values (see online version for colours)

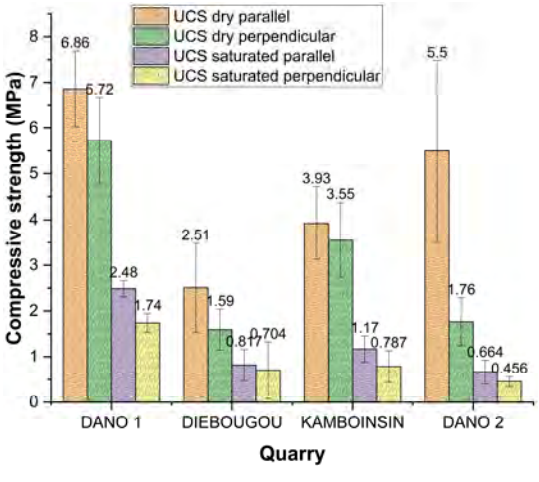

Considering the standard deviation values, Figure 12 shows that LS from Dano 1 has the highest UCS values, followed by Kamboinsin, Dano 2, and Diébougou. The tendency follows the same arrangement as the absolute dry density from quarry to another. However, it should be noted that the stones from Dano 2 that present coarse macropores present a relatively high standard deviation value for the series measured in a parallel

direction in a dry state. That ought to be about the quantity and distribution of macropores. Between values for the dry state and those for the saturated state, 56% and 88% of the compressive strength are lost. Table 4 synthesises the variation values.

Furthermore, it can be observed that the UCS values for a load applied in the direction parallel to the anisotropy plan are lower than the UCS in the perpendicular direction regarding the anisotropy plans. Even if most studies on LS do not specify the direction and the loaded face, similar results, as mentioned previously, the difference or UCS between principal and secondary direction, have been obtained for LS in India, such as in the study of Nasheed et al. (2018). For the differences and the variation range observed between UCS in dry versus UCS in saturated conditions, many studies corroborate the results shown in Figure 12 (Narayanaswamy et al., 2016; Lawane et al., 2011; Kabore et al., 2019) for laterite stone. Furthermore, some other natural stones present the same trend of resistance loss of over 20% with increased moisture content (Wong et al., 2016; Rossana and Paola, 2012). To summarise that analysis, it can be inferred that the loading direction and the moisture content affect the load-bearing capacity of the LS, and it should be an input factor for the calculation of laterite stone-based masonry structures.

For variation regarding the loading direction, average losses of 14% and 32% are observed in dry and saturated states, respectively. For the dry state, the variation for the Dano 2 quarry is considered an outlier since its integration in the analysis induces an overlapping standard deviation value. Table 5 and Table 6 present the values of the previous analysis.

Table 4 Strength loss from dry to saturated state

Quarry	*Direction*	*Variation dry/saturated*	*Mean value*	*Standard deviation*
Dano 1	Parallel	64%	71%	10%
	Perpendicular	70%		
Dano 2	Parallel	88%		
	Perpendicular	74%		
Kamboinsin	Parallel	70%		
	Perpendicular	78%		
Diebougou	Parallel	67%		
	Perpendicular	56%		

Table 5 Strength difference between perpendicular and parallel direction in dry state

Quarry	*Hydric state*	*Variation parallel/perpendicular*	*Mean value*	*Standard deviation*
Dano 1	Dry	17%	14%	4%
Dano 2		----------		
Kamboinsin		10%		
Diebougou		15%		

Figure 13 gives the tensile strength of the LS in a dry state. It shows that the flexural behaviour of the LS follows the same tendency as the compressive strength one but with relatively very low values registered. In the case of the tensile strength, there is no significant difference between the values in perpendicular and parallel directions.

Regarding the samples' dimensions for the test and the low values for the dry state, the saturated state tests could not be conducted since the values were under the minimum sensitivity value of the load sensor. Figure 14 shows that the quarry of Dano 1 has the lowest Poisson's ratio mean value (0.24), and Diebougou has the highest (0.33). Regarding the absolute dry density and the total porosity values of the LS, it can be inferred that the Poisson's ratio value is highly correlated to the absolute dry density value since the greater the density value is, the lower the Poisson's ratio value is for LS. Also, except for the very soft stone of Diebougou, it is observed that the lower the total porosity value is, the lower the Poisson's ratio is, and the mean value varies from 0.1 units for 7.0 units of total porosity. For the quarry of Diebougou, the Poisson's ratio value is close to the common values for soft materials (Huang et al., 1984), so the cohesion value for this specific quarry should be lower than the one of the others' quarry (Al-Anazi, 2008). That should explain why the LS from the Diebougou quarry partially melt when soaked in water for over two hours.

Table 6 Strength difference between the perpendicular and parallel direction in a saturated state

Quarry	*Hydric state*	*Variation parallel/perpendicular*	*Mean value*	*Standard deviation*
Dano 1	Saturated	30%	32%	3%
Dano 2		30%		
Kamboinsin		32%		
Diebougou		37%		

From the above information, it can be inferred that the loss of compressive strength is quite regular for LS when the hydric state varies.

Figure 13 Graph of indirect tensile strength (see online version for colours)

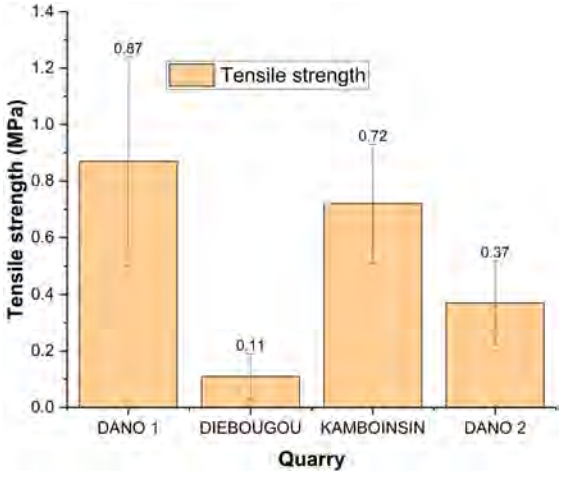

Figure 14 presents the value of Poisson's ratio based on the measurements in a dry state.

Figure 14 Chart of Poisson's ratio (see online version for colours)

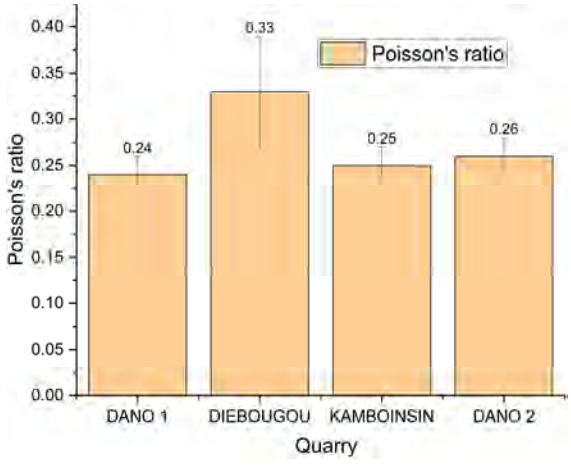

3.3 Global analysis

Figure 16 presents the strain-stress curves of LS depending on the sample size¨, the loading direction, and the hydric state for the quarry of Dano 1. It should be noted that the other quarries have quite the same tendencies as presented in Figure 16; only the maximum values differ. Table 7 gives the signification of the code used.

Table 7 Codification of the information for stress-strain curves graph

Code	*Signification*
Dry – 7 × 7 samples	The mean curve of a 7 × 7 × 7 centimetres cubic shape sample in a dry state loaded in a direction parallel to anisotropy plans
Saturated – 7 × 7 samples	The mean curve of 7 × 7 × 7 centimetres cubic shape samples in a saturated state loaded in a direction parallel to anisotropy plans
Dry – 14 × 14 samples	The mean curve of 14 × 14 × 14 centimetres cubic shape samples in a dry state loaded in a direction parallel to anisotropy plans

Figure 15 presents the graph of the stress-strain curves regarding sample size and hydric state of all the quarries studied. It gives a general view of the trends and the variations in the mechanical behaviour. To better appreciate the differences in the quarries, Figure 16, Figure 17, Figure 18, and Figure 19 give a zoomed view of each quarry.

In Figure 16, Figure 17, Figure 18, and Figure 19, it is shown that the size of the LS influences the behaviour of the LS. The LS has a ductile behaviour for relatively small samples, whereas, for greater dimensions, it adopts a quasi-brittle behaviour. Furthermore, in a saturated state, it has a quasi-plastic behaviour. That is an interesting finding since, according to the literature review; the behaviours of LS-based masonry structure studies do not consider these phenomena (Nasheed et al., 2018; Narayanaswamy et al., 2016; Lawane et al., 2011; Kasthurba et al., 2008).

Figure 15 Graph of the stress-strain curves regarding sample size and hydric state for the four quarries (see online version for colours)

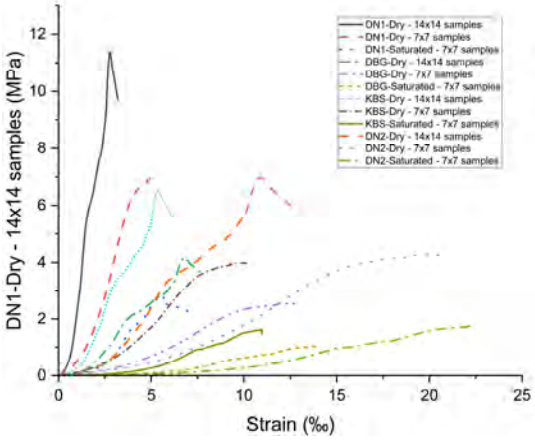

Figure 16 Graph of the stress-strain curves regarding sample size and hydric state for DANO 1 quarry (see online version for colours)

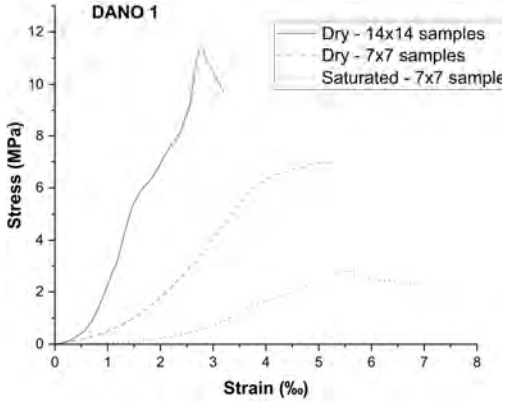

Figure 17 Graph of the stress-strain curves regarding sample size and hydric state for DIEBOUGOU quarry (see online version for colours)

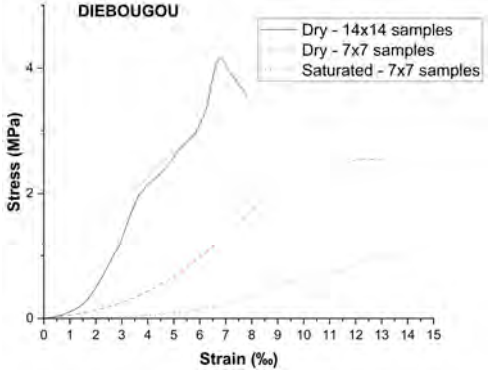

Figure 18 Graph of the stress-strain curves regarding sample size and hydric state for KAMBOINSIN quarry (see online version for colours)

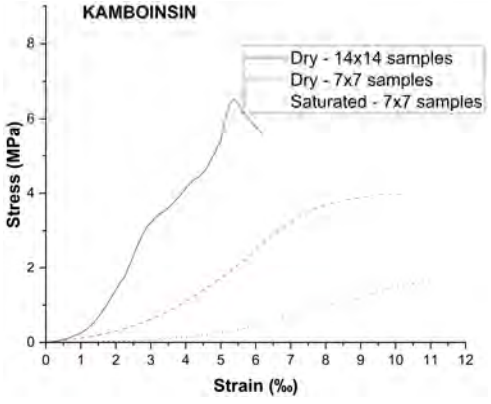

Figure 19 Graph of the stress-strain curves regarding sample size and hydric state DANO 2 quarry (see online version for colours)

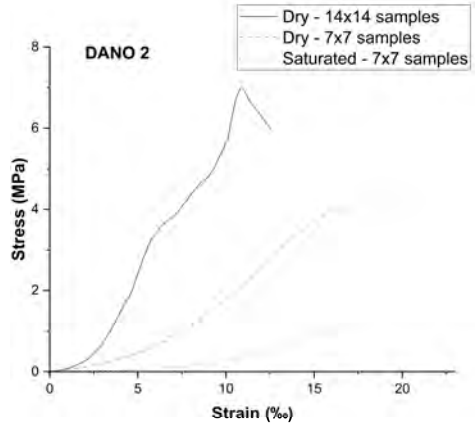

Figure 20 Strength loss due to load-unload cycles (see online version for colours)

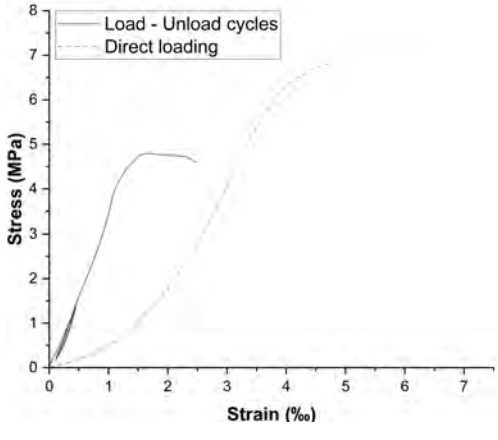

Figure 20 presents the mean stress-strain curves of the same quarry (Dano 1). One is measured including a load-unload cycle in between 10% and 30% of the expected compressive strength (test method presented in Figure 5 according to NF EN 14580, 2005), and the other one is measured directly till failure of the specimen during the compressive strength test (test method presented on Figure 5 according to NF EN 1926, 2007). The other quarries of this study follow the same tendency.

It is observed in Figure 20 that load-unload cycles cause severe compressive strength loss on the LS. In principle, the samples used to determine the elastic moduli (load-unload cycle curves) have a thickness of about twice that of the ones used for compression tests, so they should present a higher compressive strength based on the observations made in the previous paragraph. More than 22% of the compressive strength is lost after three load-unload cycles in the range presented previously. The difference between the curves' slopes should be explained by the gap regarding the thickness, as observed previously. The combination of four different phenomena may explain the loss in compressive strength by fatigue. Load-unload cycles subject the stone to repeated stress and strain, causing microscopic damage and fatigue accumulation within the material. That can lead to a gradual reduction in its overall strength.

Figure 21 Theoretical stress-strain curve for LS

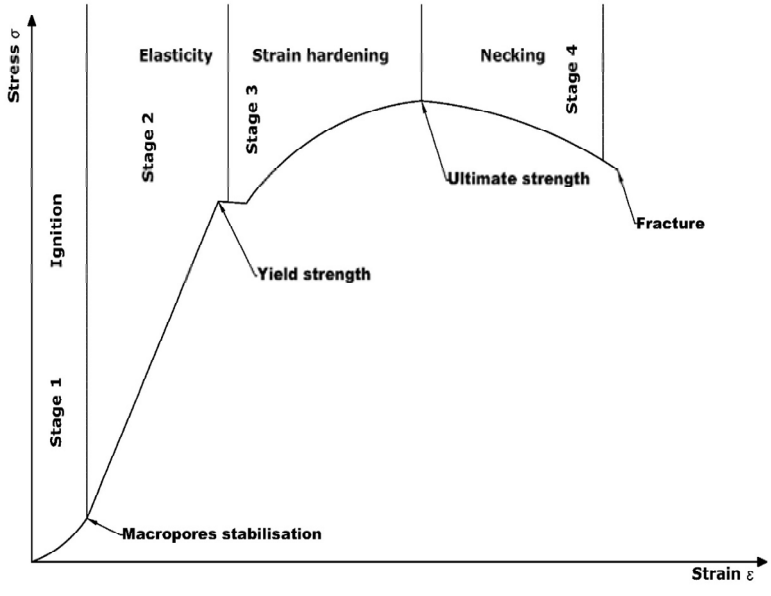

Second, the development of microcracks. These loading and unloading cycles can promote the initiation and propagation of microcracks within the LS. These microcracks act as stress concentrators, reducing the effective load-bearing capacity of the material and ultimately leading to lower compressive strength – third, stress relaxation. When a stone is subjected to load-unload cycles, it may experience stress relaxation over time. Stress relaxation refers to the phenomenon where the material gradually loses its ability to resist applied stress due to internal rearrangements of its structure (creep). That can result in a decrease in compressive strength. That is observed very often for long periods of load application time – finally, plastic deformation. Load-unload cycles can induce

plastic deformation in the stone, causing permanent changes in its shape and structure. This plastic deformation can weaken the material and reduce its compressive strength. A slope deviation in the cycle range after the second cycle is noticed on the curved cyclic load application. To synthesise, a direct loading process till failure typically applies a constant and continuous load until the stone fractures; the loading method does not involve repeated stress cycles or allow stress relaxation, microcrack propagation, or plastic deformation to occur over time. As a result, the compressive strength measured under direct loading conditions may be higher than that observed after subjecting the stone to load-unload cycles. Some authors have observed the same tendency in some other stones (Doğan and Williams, 2011; Momeni et al., 2015; Zhou et al., 2021; Chen et al., 2022).

Considering all the observations and results, it can be inferred that LS are elastoplastic materials, sometimes ductile, sometimes fragile, with a behaviour curve in compression, as presented in Figure 21.

Figure 22 Calculation factor of strain regarding the hydric state evolution of LS (see online version for colours)

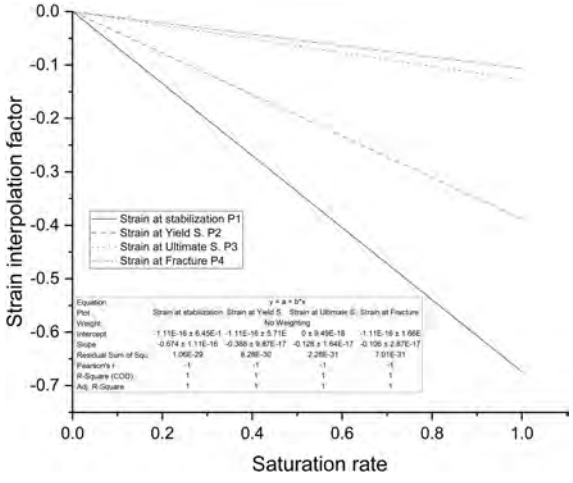

For each quarry, values of the strain and stress for each limit of each interval (stage) have been determined for the dry and saturated states on the average stress-strain curves, respectively. The representative standard deviation value is between 0.07 and 0.1, depending on the quarry. Assuming a saturation rate of 100% for the saturated state after 48 hours of immersion, the evolution trend of the saturation process transforms the dry state curve linearly into the saturated state curve. Since the highlighted stages present common trends regarding the stages in the dry state compared to the saturated state, determining interval limits is sufficient to approximate the stress-strain curves for each saturation rate from 0% (dry) to 100% (saturated). The mechanical properties parameters in compression can quite accurately be determined based on the characterisation values of the dry or saturated state. This approach is important because the LS in masonry structures in their environment has a hydric state varying between the dry and saturated states and never reaching the extremum values. From these results, the variations in the mechanical properties regarding the moisture content of the LS could be computed, leading to quite accurate and consistent results in dimensioning LS-based masonry

structures, so numerical approaches should be more useful instead of the empirical formulas for masonry structures with LS Figure 22 and Figure 23 present the evolution trend of the strain and stress for each interval limit.

Figure 23 Calculation factor of stress regarding the hydric state evolution of LS (see online version for colours)

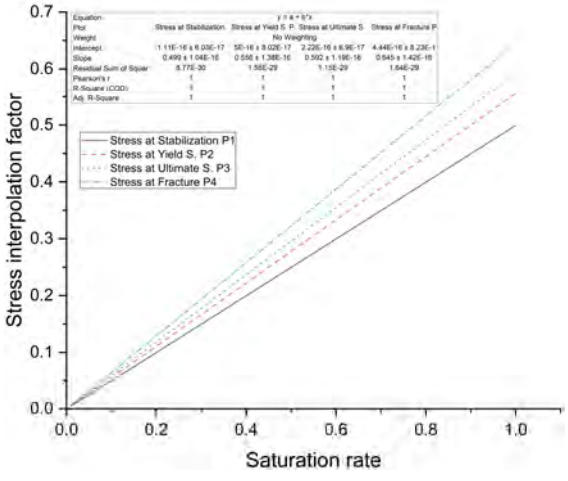

Table 8 Input values for the statistical analysis

Quarry	*DN1*	*DN2*	*KBS*	*DBG*
PRD	6.86	5.5	3.93	2.51
PPD	5.72	1.76	3.55	1.59
PRS	2.48	0.66	1.17	0.82
PPS	1.74	0.46	0.79	0.7
CPDS1	7.1	20.96	9.77	45.72
CPDS2	8.03	9.7	10.87	47.35
TPOR	23.75	38.5	30.65	19.32
OPOR	18.97	21	26.71	22.7
ADD	28.04	26.16	25.83	22.37
ITS	0.87	0.37	0.72	0.11
YMDS1	3345	1156	4480	1732
YMDS2	8370	2137	4332	3401

From the curves, the stress and strain are obtained through the following formulas;

$$\begin{cases} \varepsilon_{\%sat} = \varepsilon_d \times (1-\alpha) \\ \sigma_{\%sat} = \sigma_d \times (1-\beta) \end{cases} \tag{4}$$

where $\begin{cases} \varepsilon_{\%sat} \text{ is the strain corresponding to the saturation rate considered} \\ \varepsilon_d \text{ is the strain corresponding to the dry state of the specimen} \\ \alpha \text{ is the value read on the corresponding evolution curve} \end{cases}$, and

$\begin{cases} \sigma_{\%sat} \text{ is the stress corresponding to the saturation rate considered} \\ \sigma_d \text{ is the stress corresponding to the dry state of the specimen} \\ \beta \text{ is the value read on the corresponding evolution curve} \end{cases}$.

Figure 24 Scatter plots of the parameters two by 2

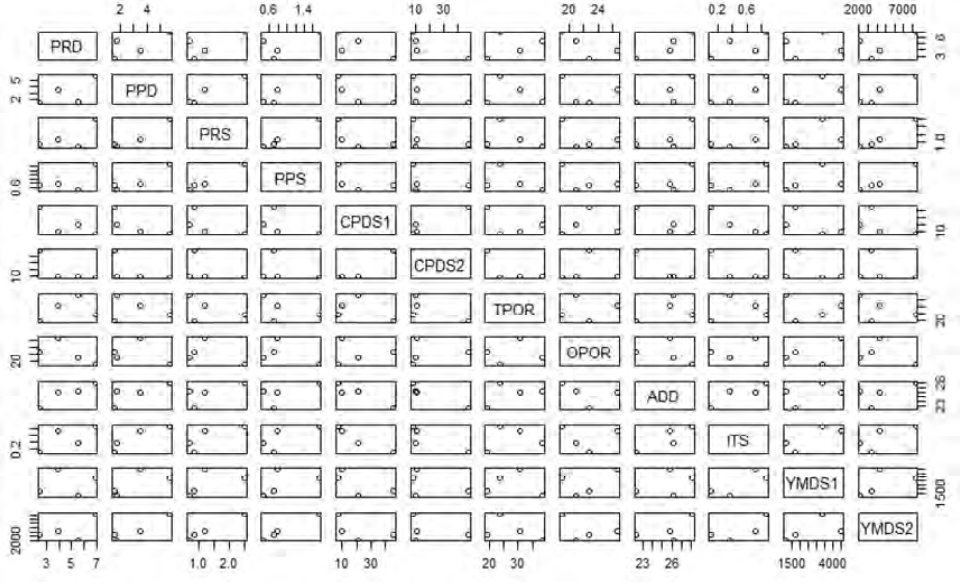

The results show that water saturation causes a significant loss of strength and increased deformability in the laterite stone. These findings are consistent with the previous study on some so-called similar stones (Mann and Fatt, 1960; Shakoor and Barefield, 2009; Verstrynge et al., 2014). Compressive strength and elastic modulus losses can be attributed to two distinct causes that may have occurred concurrently. The first reason could be that the surface energy of the crack boundaries decreases when the pore is filled with water (Rabat et al., 2020). In other words, moisture reduces the distribution of free surface energy, facilitating the proliferation of microcracks by decreasing the mechanical property values. About Lawane Gana (2014) gives the mineral composition of LS from quarries similar to the ones of this study; considering the explanations in Morin and Todor (1975), Robinet et al. (1999) and Wesley (2010) and combined with the observations made when conducting the tests, it can be inferred that all the quarries studied here do no content significant expansive clay mineral rates. Following the previous observations, the second explanation could be the reawakening of cementation between grains caused by solution or dispersion since no expansive clays in LS could induce fissure formation.

Figure 25 (a) Graph of variables for the first factorial plan and (b) Graph of individuals for the first factorial plan

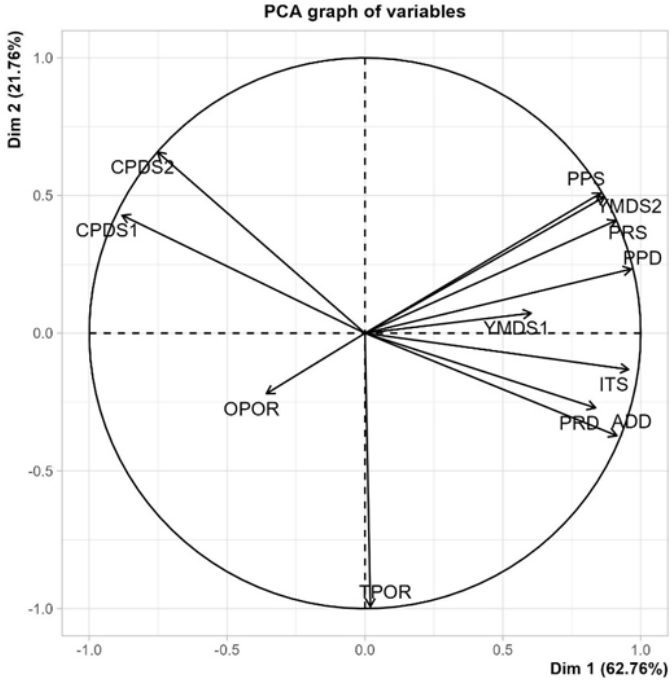

(a)

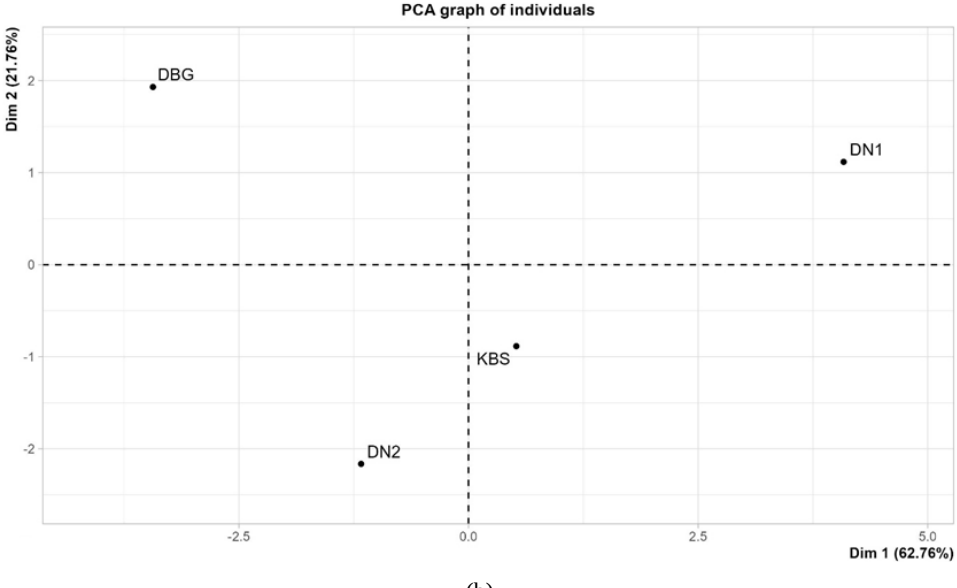

(b)

Figure 26 (a) Graph of variables for the second factorial plan and (b) Graph of individuals for the second factorial plan

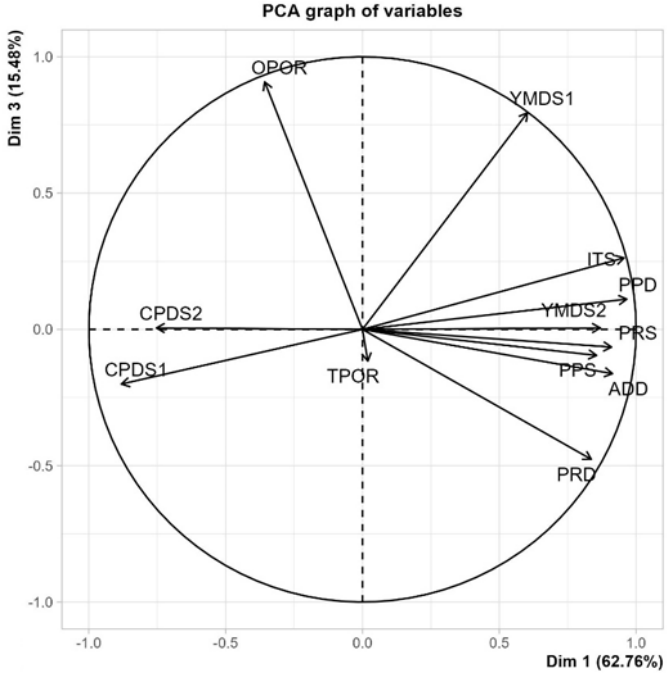

(a)

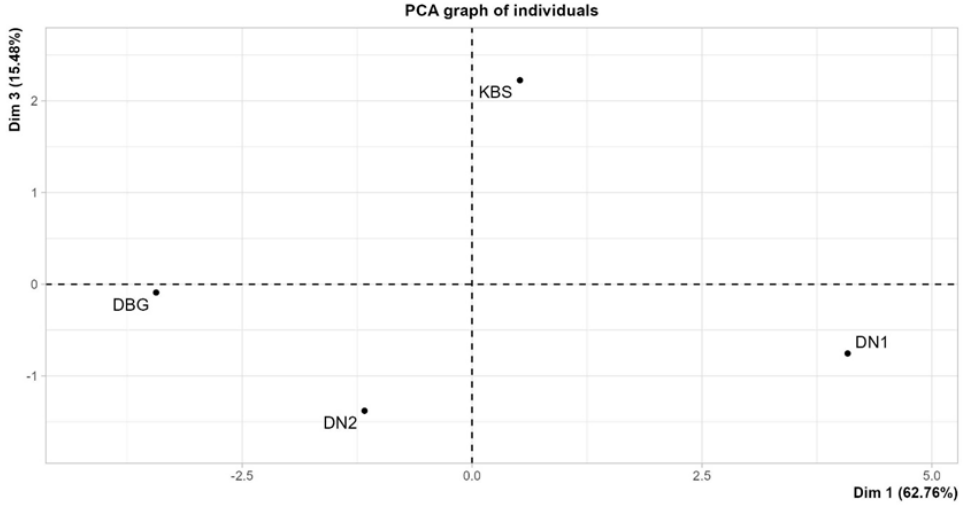

(b)

Table 8 presents the results input for the statistical analysis.

The codification is explained in Table 2 and Table 3.

The analysis of the graphs does not detect any outliers. The inertia of the first dimensions shows if there are strong relationships between variables and suggests the

number of dimensions that should be studied. The first two dimensions of analysis express 84.52% of the total dataset inertia; that means that the plane explains 84.52% of the individuals' (or variables') total cloud variability.

Figure 24 presents the scatter plot two by two of the studied parameters. It highlights a relative linear correlation between some of the variables. For example, compression and tensile strength correlate to absolute dry density, whereas young moduli and capillary pore size correlate to total and open porosity. From Figure 25 and Figure 26, it can be inferred that the studied quarries represent the existing LS since, in Figure 25(b), there is at least one quarry on each quadrant. Regarding the first factorial plan that presents over 83% of the information, each quadrant resumes some similar properties such as pore diameter for the first one, compression strength and moduli for the second, tensile strength and density for the third and porosity for the fourth. LS gather on some properties and differ on others according to the second factorial plan. Dano 1 is a dense, resistant stone with very poor porosity and low pore diameter. Kamboinsin has the second-best mechanical properties and higher porosity values than Dano 1. It represents the best compromise between mechanical and physical properties. Dano 2 follows and is the most porous stone in this study. Diebougou presents the weakest mechanical properties but has a higher pore diameter.

4 Conclusions

This study aimed to set methods and equations for assuming the stress and strain in laterite stone considering the water saturation rate and the size of the stone. To achieve this aim, experiments were conducted to determine the main mechanical and physical properties of the laterite stone, compare the results, and analyse the influence of the size of the LS and its moisture content.

Mechanical characteristics of the examined stones were reduced by over 55% on average following water saturation. Dano 1 has the highest density and UCS values (28.04 kN/m^3 and 6.36 MPa, respectively). Regarding the losses in UCS, Dan0 2 lost over 70% of its strength when saturated. The results have shown that the closer the capillary pore diameter ratio between perpendicular and parallel directions is to 1.00, the less the LS strength loss ratio is.

Under dry and saturated circumstances, significant relationships were discovered between physical and mechanical properties. These correlations, regarding the observed trends in variation between dry and saturated states, allow the indirect prediction of the behaviour depending on the hydric state, whether in a dry, intermediate, or saturated state. It also allows the prediction of the durability of stone materials and the optimisation of the quarry selection of the most suitable stone type when it is expected that they will be exposed to damp environments during their lifetime. Moreover, the behaviour change depending on the size of the LS or the hydric state has been highlighted and explained. Furthermore, novel correlation functions between the most relevant mechanical and physical were discovered for LS under dry and saturated circumstances. The resulting functions offer an alternative to mechanical laboratory experiments' time-consuming and costly development to determine UCS and moduli indirectly. It offers completion for and approaches for the numerical study of LS masonry structures, including the variation of

the saturation state. Besides numerical studies to come, the effect of weathering cycles will be addressed in further studies.

References

Al-Anazi, B.D. (2008) 'Prediction of apparent cohesion, angle of internal friction and Poisson's ratio of various types of rocks using laboratory measured unconfined (uniaxial) compressive strength', in *GEO 2008*, European Association of Geoscientists & Engineers, p.246.

Cassagnabère, F., Lachemi, M., Mouret, M. and Escadeillas, G. (2011) 'Caractérisation performantielle d'un liant ternaire à base de ciment, laitier et métakaolin', *Canadian Journal of Civil Engineering*, August, Vol. 38, No. 8, pp.837–848, DOI: 10.1139/l11-043.

Chen, Q., Cui, D., Liu, Q. and Tao, X. (2022) 'Effect of local cyclic loading on direct shear strength characteristics of shear-zone soil', *Applied Sciences (Switzerland)*, Vol. 12, No. 24, DOI: 10.3390/app122413024.

D5550-6 (2015) *Standard Test Method for Specific Gravity of Soil Solids by Gas Pycnometer*, ASTM International. American Society for Testing and Materials, January, pp.1–5.

Doğan, N. and Williams, D. (2011) 'Investigating the effect of cyclic loading on the indirect tensile strength of rocks', *Rock Mech. Rock. Eng.*, May, Vol. 45, DOI: 10.1007/s00603-011-0209-7.

Gong, F., Jacobsen, S., Li, P., Wang, Z., Maekawa, K. and Koniorczyk, M. (2022) 'Modeling of path-dependent phase change in sorption and freezing of pore water for cementitious materials', *Journal of Building Engineering*, October, Vol. 57, DOI: 10.1016/j.jobe.2022.104969.

Gong, F., Zhang, D., Sicat, E. and Ueda, T. (2014a) 'Empirical estimation of pore size distribution in cement, mortar, and concrete', *Journal of Materials in Civil Engineering*, July, Vol. 26, No. 7, DOI: 10.1061/(asce)mt.1943-5533.0000945.

Gong, F., Zhi, D., Zhou, Y., Zeng, Q. and Wang, Z. (2022b) 'Empirical modeling of pore size distribution for rock materials with its impact on pore water freezing', *Cold Reg. Sci. Technol.*, September, Vol. 201, DOI: 10.1016/j.coldregions.2022.103619.

Huang, Y.H., Lin, C. and Rose, J.G. (1984) 'Asphalt pavement design: highway versus railroad', *J. Transp. Eng.*, Vol. 110, No. 2, pp.276–282.

Kabore, M., Lawane, A., Sawadogo, C., Lo, M., Messan, A. and Pantet, A. (2019) 'Études expérimentales du comportement mécanique sous charges verticales des maçonneries en Blocs de Latérite Taillée (BLT)', *Afrique Science*, Vol. 15, No. 1, pp.201–213.

Kasthurba, A.K., Santhanam, M. and Achyuthan, H. (2008) 'Investigation of laterite stones for building purpose from Malabar region, Kerala, SW India – chemical analysis and microstructure studies', *Constr. Build Mater.*, December, Vol. 22, No. 12, pp.2400–2408, DOI: 10.1016/j.conbuildmat.2006.12.003.

Kasthurba, A.K., Santhanam, M. and Mathews, M.S. (2007) 'Investigation of laterite stones for building purpose from Malabar region, Kerala state, SW India – Part 1: field studies and profile characterization', *Constr. Build. Mater.*, January, Vol. 21, No. 1, pp.73–82, DOI: 10.1016/j.conbuildmat.2005.07.006.

Lawane Gana, A. (2014) *Caractérisation des matériaux latéritiques indurés pour une meilleure utilisation dans l'habitat en Afrique*, International Institute for water and Environmental Engineering.

Lawane, A., Pantet, A., Vinai, R. and Thomassin, J.H. (2011) 'Etude géologique et géomécanique des latérites de Dano (Burkina Faso) pour une utilisation dans l'habitat', *Les Annales BTP*, Vol. 86, No. 16, pp.15–23.

Mann, R.L. and Fatt, I. (1960) 'Effect of pore fluids on the elastic properties of sandstone', *Geophysics*, Vol. 25, No. 2, pp.433–444.

Momeni, A., Karakus, M., Khanlari, G.R. and Heidari, M. (2015) 'Effects of cyclic loading on the mechanical properties of a granite', *International Journal of Rock Mechanics and Mining Sciences*, Vol. 77, pp.89–96, DOI: 10.1016/j.ijrmms.2015.03.029.

Morin, W.J. and Todor, P.C. (1975) *Laterite and Lateritic Soils and other Problem Soils of the Tropics*, Agency for International Development.

Narayanaswamy, A. et al. (2016) 'Physical, mechanical and hygrothermal properties of lateritic building stones (LBS) from Burkina Faso', *Constr. Build. Mater.*, Vol. 125, pp.731–741, DOI: 10.1016/j.conbuildmat.2016.08.082ï.

Nasheed, M., Junaid Mk, M., Sreevidya, V. and Preethi, R. (2018) *Case Study on Comparison between Laterite Stone and Concrete Block*, Vol. 3, No. 2, pp.81–88.

Nasheed, M., Junaid Mk, M., Sreevidya, V. and Preethi, R. (2018) 'Case study on comparison between laterite stone and concrete block', *International Journal of Latest Engineering and Management Research (IJLEMR)*, Vol. 3, No. 2(S), pp.81–88.

Ndzié Mvindi, A.T., Onana, V.L., Ngo'o Ze, A., Ohandja, H.N. and Ekodeck, G.E. (2017) 'Influence of hydromorphic conditions in the variability of geotechnical parameters of gneiss-derived lateritic gravels in a savannah tropical humid area (Centre Cameroon), for road construction purposes', *Transportation Geotechnics*, September, Vol. 12, pp.70–84, DOI: 10.1016/j.trgeo.2017.08.003.

NF EN 12372 (2022) 'Méthodes d'essai pour pierres naturelles – Détermination de la résistance à la flexion sous charge centrée', *AFNOR EDITIONS*, Comité Européen de Normalisation, pp.1–22, March.

NF EN 13373 (2020) 'Méthodes d'essai pour pierres naturelles – Détermination des dimensions et autres caractéristiques géométriques', *AFNOR EDITIONS*, Comité Européen de Normalisation, pp.1–40, January.

NF EN 13755 (2008) 'Méthodes d'essai pour pierres naturelles – Détermination de l'absorption d'eau à la pression atmosphérique', *AFNOR EDITIONS*, Comité Européen de Normalisation, pp.1–9, August.

NF EN 14580 (2005) 'Méthodes d'essai des pierres naturelles – Détermination du module d'élasticité statique', *AFNOR EDITIONS*, Comité Européen de Normalisation, pp.1–14, August.

NF EN 1925 (1999) 'Méthodes d'essai pour pierres naturelles – Détermination du coefficient d'absorption d'eau par capillarité.', *AFNOR EDITIONS*, Comité Européen de Normalisation, pp.1–12, July.

NF EN 1926 (2007) 'Méthodes d'essai des pierres naturelles – Détermination de la résistance en compression uniaxiale', *AFNOR EDITIONS*, Comité Européen de Normalisation, pp.1–20, April.

NF EN 1936 (2007) 'Méthodes d'essai des pierres naturelles – Détermination des masses volumiques réelle et apparente et des porosités ouvertes et totale', *AFNOR EDITIONS*, Comité Européen de Normalisation, pp.1–12, May.

NF EN 771-6 + A1 (2015) 'Spécifications pour éléments de maçonnerie – Partie 6 : éléments de maçonnerie en pierre naturelle', *AFNOR EDITIONS*, Comité Européen de Normalisation, Bruxelles, pp.1–37, October.

NF EN 772-1 + A1 (2015) 'Méthodes d'essai des éléments de maçonnerie – Partie 1 : détermination de la résistance à la compression', *AFNOR EDITIONS*, Comité Européen de Normalisation, pp.1–15, December.

NF EN 772-11 (2011) 'Méthodes d'essai des éléments de maçonnerie – Partie 11 : détermination de l'absorption de l'eau par capillarité des éléments de maçonnerie en béton de granulats, en béton cellulaire autoclavé, en pierre reconstituée et naturelle et du taux initial d'absorption d'eau des éléments de maçonnerie en terre cuite', *AFNOR EDITIONS*, Comité Européen de Normalisation, pp.1–10, July.

NF EN 772-16 (2011) 'Méthodes d'essai des éléments de maçonnerie – Partie 16 : détermination des dimensions', *AFNOR EDITIONS*, Comité Européen de Normalisation, pp.1–15, August.

Oguchi, C.T. and Yu, S. (2021) 'A review of theoretical salt weathering studies for stone heritage', *Progress in Earth and Planetary Science*, 1 December, Vol. 8, No. 1, Springer Science and Business Media Deutschland GmbH, DOI: 10.1186/s40645-021-00414-x.

Oyelami, C.A. and Van Rooy, J.L. (2016) 'A review of the use of lateritic soils in the construction/development of sustainable housing in Africa: a geological perspective', *Journal of African Earth Sciences*, 1 July, Vol. 119, pp.226–237, Elsevier Ltd., DOI: 10.1016/j.jafrearsci.2016.03.018.

Přikryl, R. (2013) 'Durability assessment of natural stone', *Quarterly Journal of Engineering Geology and Hydrogeology*, Vol. 46, No. 4, pp.377–390, DOI: 10.1144/qjegh2012-052.

Rabat, A., Cano, M. and Tomás, R. (2020) 'Effect of water saturation on strength and deformability of building calcarenite stones: correlations with their physical properties', *Constr. Build. Mater.*, January, Vol. 232, DOI: 10.1016/j.conbuildmat.2019.117259.

Robinet, J.C., Pakzad, M., Jullien, A. and Plas, F. (1999) 'A general modelling of expansive and non-expansive clays', *Int. J. Numer. Anal. Methods Geomech.*, Vol. 23, No. 12, pp.1319–1335.

Rossana, B. and Paola, M. (2012) 'The effect of water on the strength of building stones', *American Journal of Environmental Sciences*, Vol. 8, No. 2, p.158.

Shakoor, A. and Barefield, E.H. (2009) 'Relationship between unconfined compressive strength and degree of saturation for selected sandstones', *Environmental & Engineering Geoscience*, Vol. 15, No. 1, pp.29–40.

Sun, X., Wang, S., Jin, J., Wang, Z. and Gong, F. (2023) 'Computational methods of mass transport in concrete under stress and crack conditions: a review', *Journal of Intelligent Construction*, June, Vol. 1, No. 2, p.9180015, DOI: 10.26599/jic.2023.9180015.

Török, Á. and Vásárhelyi, B. (2010) 'The influence of fabric and water content on selected rock mechanical parameters of travertine, examples from Hungary', *Eng. Geol.*, October, Vol. 115, Nos. 3–4, pp.237–245, DOI: 10.1016/j.enggeo.2010.01.005.

Verstrynge, E., Adriaens, R., Elsen, J. and Van Balen, K. (2014) 'Multi-scale analysis on the influence of moisture on the mechanical behavior of ferruginous sandstone', *Constr Build Mater*, Vol. 54, pp.78–90, https://doi.org/10.1016/j.conbuildmat.2013.12.024.

Washburn, E.W. (1921) 'The dynamics of capillary flow', *Physical Review*, March, Vol. 17, No. 3, pp.273–283, DOI: 10.1103/PhysRev.17.273.

Wesley, L.D. (2010) *Geotechnical Engineering in Residual Soils*, pp.115–133, John Wiley & Sons, Ltd., Haboken, New Jersey, https://doi.org/https://doi.org/10.1002/9780470943113.ch6.

Wong, L.N.Y., Maruvanchery, V. and Liu, G. (2016) 'Water effects on rock strength and stiffness degradation', *Acta Geotechnica*, 1 August, Vol. 11, No. 4, pp.713–737, Springer Verlag, DOI: 10.1007/s11440-015-0407-7.

Zhou, Y., Zhao, D., Li, B., Wang, H., Tang, Q. and Zhang, Z. (2021) 'Fatigue damage mechanism and deformation behaviour of granite under ultrahigh-frequency cyclic loading conditions', *Rock Mech. Rock. Eng.*, Vol. 54, No. 9, pp.4723–4739, DOI: 10.1007/s00603-021-02524-w.